Published in final edited form as:
Opt Lett. 2012 March 1; 37(5): 872–874.

Dual Modality Photothermal Optical Coherence Tomography and Magnetic Resonance Imaging of Carbon Nanotubes

Jason M. Tucker – Schwartz[1], **Tu Hong**[2], **Daniel C. Colvin**[3], **Yaqiong Xu**[2], and **Melissa C. Skala**[1,*]

[1]Department of Biomedical Engineering, Vanderbilt University, VU Station B Box 351631, Nashville TN, 37235

[2]Department of Electrical Engineering and Computer Science, Vanderbilt University, 2301 Vanderbilt Place, Nashville TN, 37235

[3]Department of Radiology and Radiological Sciences, Vanderbilt University, 1161 21st Ave South, Medical Center North, Nashville TN, 37232

Abstract

We demonstrate polyethylene glycol coated single-walled carbon nanotubes (CNTs) as contrast agents for both photothermal optical coherence tomography (OCT) and magnetic resonance imaging. Photothermal OCT was accomplished with a spectral domain OCT system with an amplitude modulated 750 nm pump beam using 10 mW of power, and T_2 MR imaging was achieved with a 4.7 T animal system. Photothermal OCT and T_2 MR imaging achieved sensitivities of nM concentrations to CNTs dispersed in amine terminated polyethylene glycol, thus establishing the potential for dual-modality molecular imaging with CNTs.

Preclinical molecular imaging of cancer has the potential to increase the understanding of fundamental cancer biology, elucidate mechanisms of cancer treatment resistance, and increase effectiveness of drug candidates. Imaging tools used for studying the molecular expression of cancer include PET, SPECT, MRI, photoacoustics, and a number of optical imaging techniques. Each imaging method provides unique levels of sensitivity, depth penetration, and resolution. MRI can provide better spatial resolution anatomical images than nuclear imaging with the ability to extract additional functional information including blood flow and cellularity. However, MRI suffers from poor sensitivity to molecular contrast agents and poor resolution compared to microscopic optical imaging techniques.

Optical coherence tomography (OCT) holds a specialized niche in optical imaging, providing structural information at high resolution (~1–10 μm) with deep optical image penetration (1–3 mm). Recently, functional imaging instrumentation and dynamic contrast agents have expanded the abilities of OCT to image collagen using second harmonics [1], paramagnetic contrast agents using magnetomotive displacements for combined OCT/MRI studies [2], and plasmon resonant particles both due to increased backscattering [3] and photon absorption [4–6]. Photothermal OCT of gold nanoparticle contrast agents has been demonstrated both *in vitro* [4, 5] and *ex vivo* [6], and offers a particularly sensitive method for detecting molecular expression in biological systems. Photothermal OCT uses an amplitude-modulated laser to perturb the temperature (and therefore index of refraction) surrounding a highly absorbing contrast agent. OCT is then used to locate the contrast agent

*Corresponding author: m.skala@vanderbilt.edu.

in three dimensions, independent of the scattering background, with the potential for mapping contrast agent concentration quantitatively.

The depth of OCT imaging is shallow compared to MRI due to optical scattering and attenuation. Combining the strengths of MRI and OCT allows for both gross full body scale molecular expression as well as local cellular-resolution imaging at a site of interest (e.g. primary tumor). We present below the novel use of single-walled carbon nanotubes (CNTs) as inherent multi-modal imaging contrasts for use with both MRI and photothermal OCT.

CNTs are cylindrically assembled sheets of carbon atoms. CNTs have novel electrical, optical, and mechanical properties making them useful in a range of fields. In optics, due to efficient optical absorption and fluorescence at a range of near infrared wavelengths, CNTs have been used as both an imaging contrast agent [7, 8] as well as a phototherapy transducer for targeted destruction of cancer cells [9]. In MRI, CNTs have been demonstrated as T_2 spin dephasing contrast agents [10]. Of great importance for *in vivo* translation as a contrast, due to their unique size and aspect ratio, CNTs have been shown to efficiently target and enter cancer cells from intravenous injections, at 15% of the injected dose per gram, making them more promising vehicles for both targeted imaging and therapeutics than spherical contrasts including iron oxide nanoparticles [7, 11]. The surface functionalization chemistry of CNTs for biological targeting is well established [12], CNT safety and circulation dynamics have been demonstrated for *in vivo* chronic animal studies [9, 11], and nanotubes can be filled with or coated in contrasts which increase their optical and MR contrast capabilities including ICG [8] and gadolinium [13], respectively. Here, we demonstrate the potential of CNTs as inherent optical absorption and magnetic resonance dual modality contrast agents with photothermal OCT and MRI, respectively.

Single-walled CNTs (HiPCO), with a typical diameter of 1 nm and length of 100 to 400 nm, were noncovalently coated and dispersed in amine terminated polyethylene glycol (PEG) solution according to established protocols [12]. Amine terminated PEG was chosen as the surfactant due to its use in surface functionalization chemistry and impact in biocompatibility and circulation time, making the nanotubes analyzed in this paper the precursor to functionalized particles to be used in targeted biological applications. The optical extinction spectrum of the CNT sample was acquired with a spectrophotometer (Cary 5000) from 400 to 1350 nm [Fig 1(a)]. Spectrophotometry indicated broadband visible and near infrared attenuation with sharp localized peaks, indicating CNTs were well dispersed and not aggregated in solution [14]. Liquid samples were prepared with concentrations ranging from 0 nM to 168 nM for analysis (calculated from mass concentration assuming 150 nm length and 170 kDa molecular weight [7]), with mass concentration of the stock solution assessed by optical density at 808 nm with extinction coefficient of 0.0465 mg l^{-1} cm^{-1} [12].

A commercial OCT system (Bioptigen Inc.) was altered for photothermal imaging. The imaging system contained an 860 nm center wavelength, 51 nm bandwidth, super luminescent diode source (axial resolution ~ 6.4 μm in air), with 8.5 μm lateral resolution and 100 μs integration time. A titanium sapphire laser served as the photothermal beam, which was fiber coupled and integrated with the OCT system via a 50/50 fiber coupler [Fig. 1(b)]. The photothermal beam was tuned to 750 nm, and amplitude modulated with a 50% duty cycle square wave at 100 Hz with a mechanical chopper, with 10 mW of power on the sample. OCT and photothermal spot sizes were roughly equal. 1000 consecutive temporal scans were acquired for each A-scan during photothermal beam amplitude modulation. Phase [Fig. 2(a)] and magnitude data was extracted from the interference data with a chirp-Z transform. Using a custom matlab file, phase data was processed with 5th order polynomial background subtraction to account for signal drift, windowed, zero padded, and Fourier

transformed in the temporal direction [Fig. 2(b)]. The photothermal signal was set as the FFT magnitude at the chopping frequency (100 Hz), and the background signal was calculated as the mean magnitude of the next highest 50 Hz of frequencies.

To test for photothermal OCT signal linearity and sensitivity, 5 μl of CNT sample was placed into a PDMS well (~150 μm thick) on a microscope slide, covered with a coverslip, and imaged with common path OCT. The photothermal OCT signal was acquired at the base of the sample. The photothermal signal was linear with concentration ($r^2 = 0.99$), and the photothermal signal was significantly higher in the lowest concentration sample (10 nM) compared to a scattering control of polystyrene microspheres with $\mu_s = 100\ cm^{-1}$ ($p<0.05$) [Fig. 2(c)]. It is important to note that the photothermal SNR increases with irradiance and chopping period, therefore the imaging sensitivity could increase with increased irradiance or decreased chopping frequency [5].

The ability of CNTs to alter native MRI contrast was assessed with a commercial 4.7 T horizontal bore animal scanner (Varian Inc.) by performing quantitative T_1 and T_2 relaxometry [Fig. 2(d)]. 200 μl CNT samples in NMR tubes were placed into a standard small animal RF coil (38 mm diameter, 33 mm length) and imaged in a 32 × 32 mm field of view with 250 μm in plane resolution and 1.5 mm slice thickness. T_1-weighted images were acquired using an inversion recovery flash imaging sequence with 5000 ms repetition time, 2.4 ms echo time, 8 degree flip angle, 16 acquisitions per inversion, and inversion times of 50, 200, 800, 2000, and 4500 ms. T_2-weighted images were collected with a multiple echo spin echo pulse sequence using 2000 ms repetition time, 6 acquisitions, 8 ms echo spacing, and 32 echoes starting at 8 ms. T_1 and T_2 maps were calculated by fitting the signal at each voxel across time to a mono-exponential model. R_1 ($\equiv 1/T_1$) and R_2 ($\equiv 1/T_2$) were calculated to generate linear concentration dependent relaxivity curves. The relaxivity (slope of the concentration curve) of CNTs was 19,945 $s^{-1}\ mM^{-1}$ for T_2 contrast and 1,152 $s^{-1}\ mM^{-1}$ for T_1 contrast. In MRI, *in vivo* sensitivity is a function of SNR and relaxivity of the tissues being imaged, although the concentration necessary to change the baseline relaxivity by 10% is a good estimate of *in vivo* sensitivity [15]. Assuming a standard tissue T_2 between 50 and 100 ms, the *in vivo* concentration of CNTs to induce a 10% change in signal, using T_2 imaging, is between 50 and 100 nM.

Two dimensional images of solid phantoms were also acquired. Low gelling temperature agarose was mixed with either water as a negative control, or CNTs to create 2% agarose gels with either 0 or 84 nM nanotube concentrations. The CNT sample was added to two 1 mm capillary tubes via capillary action and allowed to cool at 4 degrees C while covered in parafilm to avoid water evaporation. The capillary tubes were then placed across a 15 ml falcon tube through drill holes and sealed. One tube was placed near the surface of the phantom while the other tube was placed deeper in the sample. After gelling, the majority of the glass surrounding the superficial capillary tube was removed to leave a bare cylindrical agarose gel of CNTs. The 15 ml tube was then filled with 2% agarose solution until covering the superficial CNT gel, and was allowed to gel at room temperature during a 10 minute 1000 rpm centrifugation to remove air bubbles.

The phantom was imaged with photothermal OCT using the system in Fig. 1(b), with the addition of a reference arm mirror. A 1.2 mm lateral B-scan was imaged, and the final photothermal image was average filtered to decrease noise. The same phantom was then imaged with MRI, using the instrument described above. A 100 μm lateral resolution, 1.5 mm coronal slice was imaged with T_2 weighting using a multiple spin-echo pulse sequence with a repetition time of 2 s, 10 ms echo spacing, with 40 echoes, and 6 acquisitions. Phantom images [Fig. 3] confirmed both the capabilities and limitations of each imaging modality. Photothermal imaging was able to discriminate the agarose/CNT cylinder from the

scattering agarose background, while the OCT magnitude image could not [Fig. 3(a), 3(b)]. PT-OCT also allowed for high resolution targeted imaging, although to a limited depth (1.5 mm). The MR image of the phantom at the 50 ms echo indicates significant signal differences between the agarose and agarose/CNT regions of the image [Fig. 3(c)] at all depths, although with in plane resolution two orders of magnitude less than OCT. The nanotube contrast effects with MRI are greater in the image than expected according to the sensitivity curve [Fig. 2(d)], which is due to an increase in agarose concentration from water evaporation in the capillary tube sample.

We have demonstrated the ability of both MRI and photothermal OCT to distinguish CNTs from background at nM concentrations. Importantly, this concentration is approximately equivalent to that demonstrated for marking cell receptors with systemic *in vivo* delivery of CNTs [7], and much less than the theoretical [3] and *in vitro* [16] targeting capabilities of CNTs. This study has shown the ability of a common contrast agent, which is an efficient biological targeting agent, to be sensitive to both functional OCT and MR imaging, thereby enabling multi-scale multi-modality preclinical molecular imaging.

Acknowledgments

This work was supported by funding from the NIH (grant R00 CA142888) and NSF (grant EECS-1055852). The authors would also like to thank Dr. Chetan Patil and Lucas Hofmeister for useful discussions on the experiments performed.

References

1. Jiang Y, Tomov IV, Wang YM, Chen ZP. Appl Phys Lett. 2005; 86
2. John R, Rezaeipoor R, Adie SG, Chaney EJ, Oldenburg AL, Marjanovic M, Haldar JP, Sutton BP, Boppart SA. Proc Natl Acad Sci U S A. 2010; 107:8085–8090. [PubMed: 20404194]
3. Agrawal A, Huang S, Wei Haw Lin A, Lee MH, Barton JK, Drezek RA, Pfefer TJ. J Biomed Opt. 2006; 11:041121. [PubMed: 16965149]
4. Skala MC, Crow MJ, Wax A, Izatt JA. Nano Lett. 2008; 8:3461–3467. [PubMed: 18767886]
5. Adler DC, Huang SW, Huber R, Fujimoto JG. Opt Express. 2008; 16:4376–4393. [PubMed: 18542535]
6. Zhou C, Tsai TH, Adler DC, Lee HC, Cohen DW, Mondelblatt A, Wang Y, Connolly JL, Fujimoto JG. Opt Lett. 2010; 35:700–702. [PubMed: 20195324]
7. De la Zerda A, Zavaleta C, Keren S, Vaithilingam S, Bodapati S, Liu Z, Levi J, Smith BR, Ma TJ, Oralkan O, Cheng Z, Chen X, Dai H, Khuri-Yakub BT, Gambhir SS. Nat Nanotechnol. 2008; 3:557–562. [PubMed: 18772918]
8. de la Zerda A, Liu Z, Bodapati S, Teed R, Vaithilingam S, Khuri-Yakub BT, Chen X, Dai H, Gambhir SS. Nano Lett. 2010; 10:2168–2172. [PubMed: 20499887]
9. Moon HK, Lee SH, Choi HC. ACS Nano. 2009; 3:3707–3713. [PubMed: 19877694]
10. Ananta JS, Matson ML, Tang AM, Mandal T, Lin S, Wong K, Wong ST, Wilson LJ. J Phys Chem C. 2009; 113:19369–19372.
11. Liu Z, Cai W, He L, Nakayama N, Chen K, Sun X, Chen X, Dai H. Nat Nanotechnol. 2007; 2:47–52. [PubMed: 18654207]
12. Liu Z, Tabakman SM, Chen Z, Dai H. Nat Protoc. 2009; 4:1372–1382. [PubMed: 19730421]
13. Tang AM, Ananta JS, Zhao H, Cisneros BT, Lam EY, Wong ST, Wilson LJ, Wong KK. Contrast Media Mol I. 2011; 6:93–99.
14. O'Connell MJ, Bachilo SM, Huffman CB, Moore VC, Strano MS, Haroz EH, Rialon KL, Boul PJ, Noon WH, Kittrell C, Ma J, Hauge RH, Weisman RB, Smalley RE. Science. 2002; 297:593–596. [PubMed: 12142535]
15. Gore JC, Yankeelov TE, Peterson TE, Avison MJ. J Nucl Med. 2009; 50:999–1007. [PubMed: 19443583]

16. Holt BD, Dahl KN, Islam MF. Small. 2011

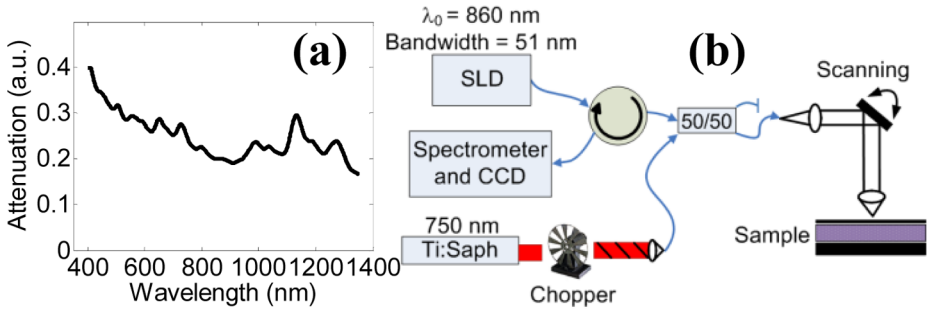

Fig. 1.

(Color Online) (a) Vis-NIR attenuation spectrum of CNTs. (b) Photothermal OCT instrumentation used for imaging (SLD = super luminescent diode source).

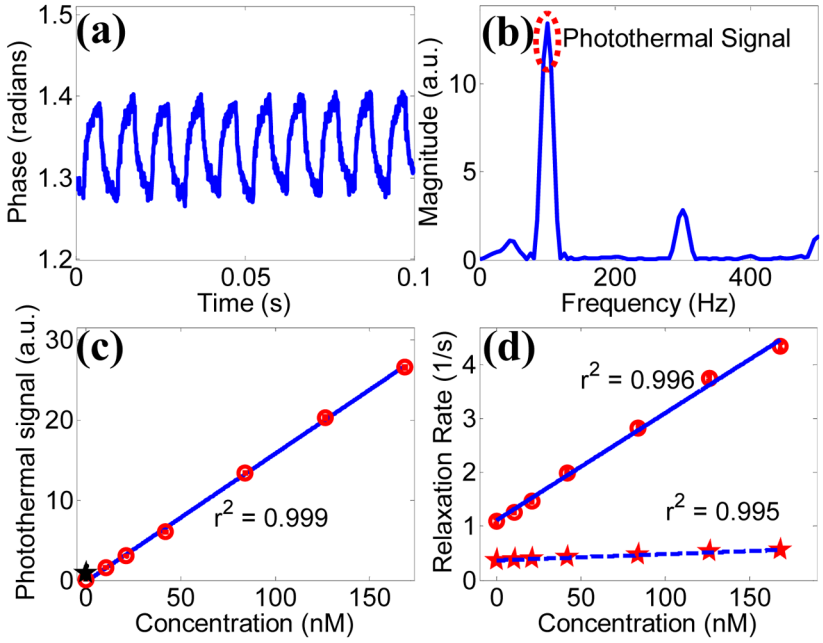

Fig. 2.

(Color online) (a) Example temporal phase data acquired from the base of 84 nM CNT phantom during photothermal modulation. (b) Fourier transform of processed phase data. (c) Photothermal signal as a function CNT concentration. The black star indicates the photothermal signal of a scattering control (μ_s = 100 cm^{-1}). (d) MRI relaxivity curves of carbon nanotubes for both T_1 (dashed) and T_2 contrast (solid).

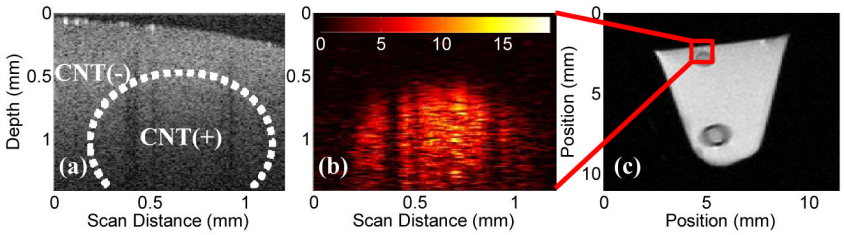

Fig. 3.

(Color online) (a) OCT magnitude image of three dimensional agarose phantom, note a lack of contrast or any visual confirmation of the presence of CNTs. CNT(+) (~84 nM) and CNT(−) regions are highlighted. (b) Photothermal OCT of the same field of view, revealing the cylindrical CNT gel inclusion. Photothermal signal is in arbitrary units. (c) Full cross sectional MRI image (50 ms echo time) of the phantom revealing both the superficial and deep CNT gel phantoms. Only the deep nanotube phantom has a capillary tube surrounding it. The dark ring surrounding the lower inclusion is due to the glass capillary tube.